A quantum symmetry preserving semiclassical method

Dmitri Babikov,[a] Robert B. Walker, and Russell T Pack
Theoretical Chemistry and Molecular Physics Group (T-12, MS B268), Theoretical Division of Los Alamos National Laboratory, Los Alamos, New Mexico 87545

(Received 29 July 2002; accepted 20 August 2002)

Symmetry constraints are built into a semiclassical propagation scheme. It is then applied to treat $H+Ne_2$ collisions at 30 K, where quantum selection rules restrict the final rotational states of symmetric Ne_2 molecules to the even manifold. The cross sections for state-to-state transitions are calculated for symmetric and nonsymmetric isotopic compositions of Ne_2. All bound and long-lived quasibound (trapped behind the centrifugal barrier) states of Ne_2 are considered. This semiclassical method captures symmetry effects and shows satisfactory agreement with the quantum results.
 [DOI: 10.1063/1.1513457]

I. INTRODUCTION

Most semiclassical methods for molecular collisions give results that violate symmetry selection rules. In this article we demonstrate a way to maintain the quantum property of symmetry using semiclassical methods. For transparency, we use the simplest version of the semiclassical method proposed by Heller and known as the frozen Gaussian wave packets method.[1] Nevertheless, our approach is general and it is straightforward to use it with more sophisticated and accurate semiclassical methods, such as the Herman–Kluk (HK) propagator,[2–10] which is also known as the semiclassical initial value representation (SC-IVR) method,[11–20] or the recently proposed coupled coherent states (CCS) method.[21–24] Here we mention that the earlier classical S-matrix theory of McCurdy and Miller[25] has been shown to describe rotational symmetry effects correctly. It is, nevertheless, important to demonstrate how modern wave-packet-based semiclassical methods may be used to treat symmetry properly.

Our interest in this problem has been driven by the long-standing puzzle of the anomalous large isotope effect[26,27] in ozone formation. There is a hypothesis[28,29,30] that molecular symmetry plays an important role in this phenomenon. Ozone is formed in the following recombination reaction,

$$O+O_2+M\leftrightarrow O_3+M. \tag{1}$$

Here the third body M may be any atmospheric atom or molecule. Different isotopes of oxygen (^{16}O, ^{17}O, and ^{18}O) may participate in this reaction and form symmetric or nonsymmetric reactant O_2 and/or product O_3 molecules. Because this process involves at least four heavy atoms, it is too complex to treat with full quantum mechanics. Classical mechanics, on the other hand, does not allow us to incorporate symmetry constraints rigorously (bins do not work properly), and this may be a reason why classical trajectory studies[31] have failed to account for anomalous isotope effects. Semiclassical methods, being somewhat intermediate between classical and quantum mechanics, are known for their relative efficiency and ability to reproduce various quantum properties.[32–38] That is why we want to develop a semiclassical method to describe symmetry effects in recombination reactions, such as the ozone recombination reaction above.

For the present study, we have chosen a simpler recombination reaction,

$$Ne+Ne+H\leftrightarrow Ne_2+H. \tag{2}$$

This choice was made to take advantage of several features.

(a) Because the Ne_2 molecule is weakly bound, its rovibrational spectrum is very simple (see Appendix A).
(b) Because, with the model mass we chose for H (see later), there are no NeH bound states, we automatically exclude the possibility of the chaperon (bound complex) recombination mechanism.[39]
(c) By choosing different isotopes of the Ne atom (^{16}Ne, ^{17}Ne, ^{18}Ne or ^{20}Ne), we can form various symmetric and nonsymmetric Ne_2 molecules and study how symmetry affects this recombination reaction.
(d) This reaction was already studied by some of us[40,41] with an approximate quantum mechanical method (VRIOSA) and this earlier study provides an opportunity to test the semiclassical method.

II. RESULTS OF VRIOSA

Before we discuss the semiclassical method, the central focus of this article, we decided to give the reader a flavor of symmetry effects by presenting some results for reaction (2) that we have obtained with the vibrational rotational infinite order sudden approximation (VRIOSA). The VRIOSA is an approximate quantum method and it treats symmetry rigorously. Overall, it produces semiquantitative results. The details of the method and its results for one symmetric isotopic combination of the Ne_2 molecule ($^{18}Ne^{18}Ne$) have been already reported.[40] Theoretically, it is more convenient to study the backward direction of reaction (2)—the collision of a Ne_2 molecule with an H atom producing state-to-state transitions in Ne_2 and, possibly, its dissociation [collision induced dissociation[42] (CID)]. Here we present results in

[a]Author to whom correspondence should be addressed. Electronic mail: babikov@lanl.gov

TABLE I. VRIOSA results. Cross sections (in a.u.) for state-to-state transitions in Ne_2+H collision. Total energy is 30 K. Final states are labeled by v and j, vibrational and rotational quantum numbers, respectively. Initial state was ground rovibrational state ($v=0,j=0$). Shown are results for three different isotopic compositions of the Ne_2 molecule, $^{16}Ne^{16}Ne$, $^{16}Ne^{18}Ne$, and $^{18}Ne^{18}Ne$.

Final states		Isotope combinations		
v	j	16/16	16/18	18/18
0	0	236.55	236.94	237.51
	1		0.51	
	2	89.13	88.54	89.18
	3		0.21	
	4	29.50	29.00	29.14
	5		0.33	
	6	5.66	5.44	5.53
	7		0.20	
	8	1.01	0.91	0.99
	9		0.08	
	10	0.21	0.18	0.22
	11		0.03	
	12	0.05	0.03	0.05
1	0	0.76	0.75	0.75
	1		0.01	
	2	0.33	0.32	0.32
	3		0.01	
	4	0.08	0.09	0.11
	5		0.00	
	6	0.06	0.05	0.05

which the initial state of Ne_2 is the ground rovibrational state ($v=0,j=0$), at a total energy of 30 K. In Table I we show state-to-state cross sections for transitions to all bound and quasibound states for three different isotopic combinations of the Ne_2 molecule—two symmetric combinations ($^{16}Ne^{16}Ne$, and $^{18}Ne^{18}Ne$) and one nonsymmetric combination ($^{16}Ne^{18}Ne$). As discussed in Appendix A, symmetric molecules exist only in even rotational states (a total of 11 states in Table I), while nonsymmetric molecules exist in both even and odd rotational states (a total of 20 states in Table I). Furthermore, Table I shows that different isotopic combinations have a different number of quasibound states.

For symmetric molecules only transitions between even states ($j=0,2,4,...$) are allowed. For nonsymmetric molecule transitions into both even and odd states ($j=0,1,2,3,...$) are allowed, and one may at first think that the corresponding cross sections would vary smoothly (statistically) as a function of quantum number j. The VRIOSA results of Table I show that this is not the case. The initial state is even ($j=0$) for all isotopic combinations and cross sections for transitions into even states ($j=0,2,4,...$) change smoothly as a function of j for all isotopic combinations. Nevertheless, transitions into odd states ($j=1,3,5,...$) for the nonsymmetric molecule $^{16}Ne^{18}Ne$ exhibit cross sections often two orders of magnitude smaller! This behavior is certainly not statistical and not classical (when a classical rotator collides with an atom, a smooth continuous distribution of angular momentum is produced). In the next sections we show that a simple semiclassical method is able to reproduce the symmetry effects outlined in Table I.

III. THEORY

We use Jacobi coordinates and define $\mathbf{r}$ as the vector connecting the two nuclei of the Ne_2 molecule and $\mathbf{R}$ as the vector connecting the center-of-mass of Ne_2 with the H atom. We follow the earlier work of one of us[43] and separate the classical and quantum parts of the system: the relative atom–molecule motion follows a classical trajectory $\mathbf{R}(t)$, while the motion in the intermolecular coordinate $\mathbf{r}$ is described by a wave function $\psi(\mathbf{r},t)$ obeying the time dependent Schrödinger equation,

$$i\frac{\partial\psi(\mathbf{r},t)}{\partial t}=\left(-\frac{1}{2\mu}\Delta_{\mathbf{r}}+V(\mathbf{r},t)\right)\psi(\mathbf{r},t). \tag{3}$$

Here the time dependence of the potential is actually driven by the classical trajectory $\mathbf{R}(t)$ of relative atom–molecule motion, $V(\mathbf{r},t)\equiv V(\mathbf{r},\mathbf{R}(t))$. This approximation should work very well here because the H atom is light and fast (compared to the much heavier Ne atoms of the molecule) and its motion may therefore be described classically. Furthermore, the role of the H atom is just to impart energy into the molecule; no quantum phenomena are expected to occur in the motion of the H atom. At the same time, the quantum properties of symmetry, which we explore in this work, are associated with the Ne_2 molecule and will be properly described by the wave function $\psi(\mathbf{r},t)$ and Eq. (3).

A. Frozen Gaussian wave packets

Equation (3) is propagated semiclassically according to the frozen Gaussian wave packets method[1] of Heller. This method has been derived and discussed several times,[1,2,44,45,46] so here we just give an outline, mostly to introduce notations. Let us suppose that initially (before the collision) our molecule is in quantum eigenstate $|a\rangle$. First, an approximate semiclassical wave function $\phi_a(\mathbf{r})$ is prepared as a superposition of Gaussian wave packets,

$$\phi_a(\mathbf{r})=N\sum_n c_n G_n(\mathbf{r}). \tag{4}$$

Here N is used for normalization, and the expansion coefficients c_n are obtained by projecting Gaussian wave packets onto the initial eigenstate, $c_n=\langle a|G_n(\mathbf{r})\rangle$. Gaussian wave packets are taken in the form,

$$G_n(\mathbf{r})=\left(\frac{2\alpha}{\pi}\right)^{3/4}\exp\{-\alpha(\mathbf{r}-\mathbf{r}_n)^2+i\mathbf{p}_n\cdot(\mathbf{r}-\mathbf{r}_n)+i\gamma_n\}. \tag{5}$$

Here $\mathbf{r}_n$ and $\mathbf{p}_n$ are the position and momentum of the center of the nth Gaussian, and γ_n is its phase. These parameters are time dependent and are used to propagate $\phi_a(\mathbf{r})$ in time by propagating each of the n Gaussian wave packets independently. Positions and momenta obey Hamilton's equations of motion (classical trajectories),

$$\dot{\mathbf{r}}_n=\frac{\mathbf{p}_n}{\mu},\quad \dot{\mathbf{p}}_n=-\nabla_{\mathbf{r}}V(\mathbf{r}_n,t). \tag{6}$$

The phases are obtained by integrating the classical action,

$$\dot{\gamma}_n = \frac{\mathbf{p}_n^2}{2\mu} - V(\mathbf{r}_n, t). \tag{7}$$

The width parameter α of the wave packets is not allowed to vary in time; it is "frozen" and is set to be a real positive number. The semiclassical wave function at time t, denoted here as $\psi_a(\mathbf{r},t)$, is obtained then as a superposition of Gaussian wave packets at time t,

$$\psi_a(\mathbf{r},t) = N(t) \sum_n c_n G_n(\mathbf{r},t). \tag{8}$$

This propagation scheme is almost as simple as classical mechanics [Eq. (6)] but each trajectory possesses a phase [Eq. (7)] and contributes coherently to the total wave function in Eq. (8). This property of the semiclassical method is essential for the description of scattering, where quantum phenomena (such as rainbows) occur. For the present study it is also important that this simple semiclassical propagation scheme produces not just a bunch of trajectories, but the final wave function [Eq. (8)], an entity which may be exposed to quantum mechanical analysis. This fact, together with appropriate choice of initial conditions for the Gaussian wave packets (described in the next section), allows us to build symmetry constraints into the dynamics and to extract symmetry-related information from the final wave function.

In one of their pioneering articles on the HK-propagator,[3] Herman and Kluk stated that the method of frozen Gaussians may be considered as an approximate HK-propagator where the so called "prefactors" (normally time-dependent and obtained from monodromy analysis[2,3]) are kept constant, and that this approximation is valid when the characteristic time of the process under consideration is short. This is indeed the case for the Ne_2+H collision considered here, because the H atom is much lighter than the Ne_2 molecule and the time scale of strong interaction is about ten times shorter than the characteristic vibrational period of Ne_2. To eliminate the error accumulated during the time when Ne_2 and H approach each other (before the collision) and separate (after the collision) we use the interaction picture.[37,38,47–52] In this approach, forward propagation with the total Hamiltonian is followed by backward propagation with a channel Hamiltonian. The channel Hamiltonian in this case corresponds to an independently moving Ne_2 molecule and H atom. The potential for this Hamiltonian is obtained by removing the Ne–H interaction terms in the pairwise-additive potential[40] used here. One may also note that we renormalize the semiclassical wave function as it evolves [the coefficient $N(t)$ in Eq. (8)] and this is more a feature of the HK-propagator[3] than of the original frozen Gaussian wave packets method of Heller.[1]

B. Representation of initial eigenstates

Eigenstates $|a\rangle$ of Ne_2 are described by the usual three-dimensional wave functions corresponding to v, j, and m quantum numbers of a diatomic,

$$a_{vjm}(\mathbf{r}) = a_{vjm}(r,\theta,\varphi) = \frac{\chi_{vj}(r)}{r} Y_j^m(\theta,\varphi). \tag{9}$$

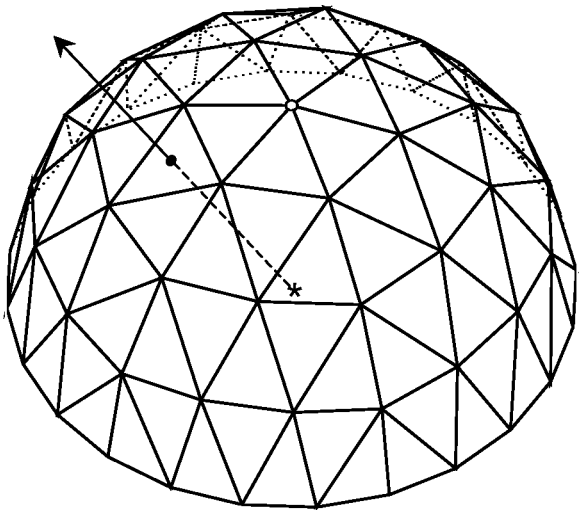

FIG. 1. Triangulation of the upper hemisphere. The North Pole is marked with an empty dot. In this particular example the triangulation gives 96 spherical triangles. One angular direction is shown as a vector starting at the center of the sphere (star) and passing through the center of surface triangle (black dot).

Here $\chi_{vj}(r)$ is vth eigenfunction of the one-dimensional radial Schrödinger equation when angular momentum number is j, and $Y_j^m(\theta,\varphi)$ is the usual spherical harmonic. As one may have noticed, the semiclassical propagation starts not from a numerically exact initial quantum eigenstate $|a\rangle$ but from an approximate (semiclassical) wave function $|\phi_a\rangle$ given by Eq. (4). Phases γ_n of all n Gaussians are taken to be zero initially. Positions $\mathbf{r}_n$ and momenta $\mathbf{p}_n$ of the Gaussian wave packets [Eq. (5)] should be properly chosen to make $|\phi_a\rangle$ a good approximation to $|a\rangle$, so that $\langle a|\phi_a\rangle \approx 1$. To describe quantum eigenstate $|a\rangle = |vjm\rangle$, we use well-known quantum-classical correspondence[53] relations and let the wave packets follow classical trajectories defined by the three following conservation laws:

$$\frac{|\mathbf{p}|^2}{2\mu} + V(\mathbf{r}) = E_{vj}, \tag{10}$$

$$|\mathbf{L}|^2 = j(j+1), \tag{11}$$

$$L_z = m. \tag{12}$$

Here E_{vj} is the rovibrational energy of the eigenstate, and $\mathbf{L} \equiv \mathbf{r} \times \mathbf{p}$ and L_z are the classical trajectory angular momentum and its z-component, respectively. Practical realization of this choice consists of the two steps described next.

First, we cover a spherical layer in space, where the wave function [Eq. (9)] is located, with Gaussians. To place Gaussians as uniformly as possible we triangulate the surface of the upper hemisphere of a polar coordinate system, as shown in Fig. 1, dividing it into spherical triangles of similar shape and approximately equal surface area. We use the centers of these triangles to define a number of angular directions, as shown in Fig. 1. The centers $\mathbf{r}_n$ of several Gaussians are placed along these directions, and, to satisfy Eq. (10), between the radial turning points. It is known, that for $j>0$ there is a part of configuration space, around the poles, where Eqs. (11)–(12) cannot be satisfied (see also Appendix B).

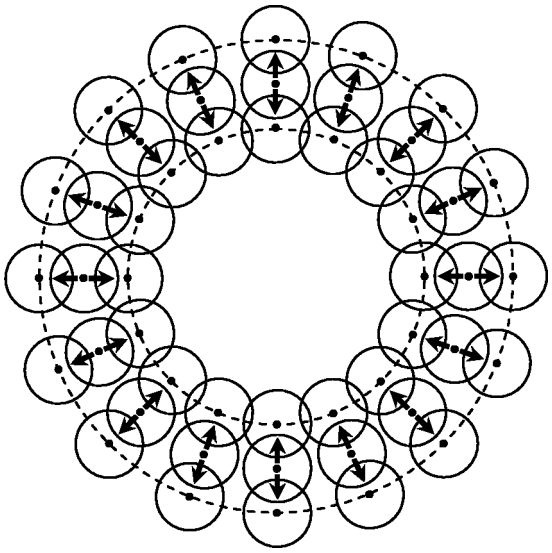

FIG. 2. Covering a spherical layer in space with Gaussians, a two-dimensional slice. Inner and outer turning points lie on dashed circles. Gaussians are shown schematically by their centers (black dots) and extend to the surrounding solid circles. Four Gaussians are placed along each radial direction: one at the inner turning point, one at the outer turning point, and two in the middle between them. In this simplest case $j=0$, so that the two Gaussians placed at the turning points have no initial momenta. The other two Gaussians have equally-valued and oppositely-directed radial momenta (bold vectors).

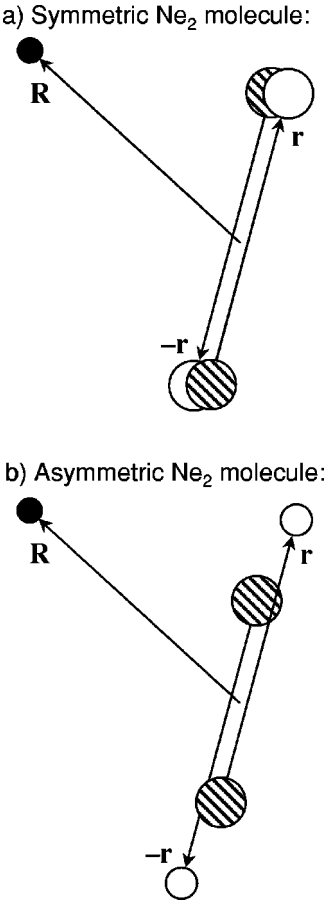

FIG. 3. Arrangements of H and Ne_2 nuclei in the case of (a) symmetric Ne_2 molecules, and (b) nonsymmetric Ne_2 molecules. See text for discussion of symmetry effects.

There, the amplitude of the wave function [Eq. (9)] is very small. For each j value this part of space is identified and is not covered by Gaussians.

Second, we assign the initial momenta $\mathbf{p}_n$ to the wave packets to obey Eqs. (10)–(12). In Appendix B it is shown that (for $j>0$) if the position $\mathbf{r}_n$ is chosen anywhere between the turning points, then four different $\mathbf{p}_n$ vectors satisfy Eqs. (10)–(12), and so we start four wave packets from each such point. If the initial position $\mathbf{r}_n$ is a turning point, then only two different $\mathbf{p}_n$ vectors satisfy Eqs. (10)–(12), and we start only two wave packets from the turning points. If $j=0$, then these are reduced to two wave packets starting from any point between the turning points and one wave packet starting from any turning point. This simplest situation is shown in Fig. 2. Here we decided to place four initial wave packets in each radial direction. Two of them start at the turning points with no initial momenta. The other two start in the middle between the turning points with equally-valued but oppositely-directed radial momenta. When $j>0$ additional tangential components of momenta appear (see Appendix B), and the picture becomes more complex.

After the upper hemisphere is covered by Gaussians, we reflect their positions and momenta through the center of the sphere onto the lower hemisphere. This finalizes the sampling procedure.

Our sampling procedure produces trajectories "on the energy shell," as opposed to Monte Carlo sampling from a Wigner space distribution.[3] We need to use "on the energy shell" trajectories, because we also want to describe the quasibound long-lived states of the Ne_2 molecule (see Appendix A) with the same procedure that we use for bound states. Classical trajectories may be prepared at the energy of a long-lived quasibound state, with appropriate initial conditions so that they remain trapped forever behind the centrifugal barrier. These trajectories permit us to reasonably describe quasibound states. On the contrary, Wigner space sampling would produce some trajectories at energies above the centrifugal barrier and allow the Ne_2 molecule to dissociate even without colliding with the H atom. These events would create a problem in the present study.

C. How do we capture the effect of symmetry?

Let us consider two wave packets placed symmetrically at the initial moment of time. We will call them the "+" and the "−" packets. This may be an arbitrarily chosen pair of symmetric wave packets from Fig. 1. They are defined by position vectors $\mathbf{r}^+=\mathbf{r}_0$ and $\mathbf{r}^-=-\mathbf{r}_0$, and momentum vectors $\mathbf{p}^+=\mathbf{p}_0$ and $\mathbf{p}^-=-\mathbf{p}_0$, respectively. These wave packets describe two different arrangements of Ne atoms in the Ne_2 molecule, as shown in Fig. 3. For the case of a *symmetric* Ne_2 molecule, where the two Ne atoms are identical, the two arrangements of the H–Ne_2 "collision complex" are also identical for any arbitrary position $\mathbf{R}(t)$ of the H atom [see Fig. 3(a)]. In this case the potential energy, which enters the equations of motion [Eq. (6)], will be exactly equal for the two wave packets: $V(\mathbf{r}^+)=V(\mathbf{r}^-)$, and the gradient vectors, entering the phase equation [Eq. (7)], will be different

just by a sign: $\nabla_{\mathbf{r}} V(\mathbf{r}^+) = -\nabla_{\mathbf{r}} V(\mathbf{r}^-)$. But for the case of a *nonsymmetric* Ne_2 molecule, where the two Ne atoms have different masses, the two arrangements of the H–Ne_2 "collision complex" are different [Fig. 3(b)], because of the slight shift in the center-of-mass of the Ne_2. As a result, the potentials and the gradients will be different for the "+" and "−" wave packets.

Let us consider first the *symmetric* case [Fig. 3(a)]. Each Gaussian wave packet is propagated independently during the collision with the H atom. Nevertheless, each pair of wave packets, placed symmetrically at the initial moment of time, will remain symmetric in its motion as the H atom evolves along its trajectory $\mathbf{R}(t)$. This is clearly seen from the equations of motion [Eqs. (6)–(7)] for the two wave packets. For the "+" wave packet we have

$$\mathbf{r}^+(t) = \mathbf{r}_0 + \int_0^t \frac{\mathbf{p}^+(t)}{\mu} dt, \tag{13}$$

$$\mathbf{p}^+(t) = \mathbf{p}_0 - \int_0^t \nabla_{\mathbf{r}} V(\mathbf{r}^+, t) dt, \tag{14}$$

$$\gamma^+(t) = \int_0^t \left[\frac{|\mathbf{p}^+(t)|^2}{2\mu} - V(\mathbf{r}^+, t) \right] dt. \tag{15}$$

For the "−" wave packet we obtain

$$\mathbf{r}^-(t) = -\mathbf{r}_0 + \int_0^t \frac{\mathbf{p}^-(t)}{\mu} dt = -\mathbf{r}_0 - \int_0^t \frac{\mathbf{p}^+(t)}{\mu} dt, \tag{16}$$

$$\mathbf{p}^-(t) = -\mathbf{p}_0 - \int_0^t \nabla_{\mathbf{r}} V(\mathbf{r}^-, t) dt = -\mathbf{p}_0 + \int_0^t \nabla_{\mathbf{r}} V(\mathbf{r}^+, t) dt, \tag{17}$$

$$\gamma^-(t) = \int_0^t \left[\frac{|\mathbf{p}^-(t)|^2}{2\mu} - V(\mathbf{r}^-, t) \right] dt = \int_0^t \left[\frac{|\mathbf{p}^+(t)|^2}{2\mu} - V(\mathbf{r}^+, t) \right] dt. \tag{18}$$

So, during the collision we will always have

$$\mathbf{r}^-(t) = -\mathbf{r}^+(t), \quad \mathbf{p}^-(t) = -\mathbf{p}^+(t), \quad \gamma^-(t) = \gamma^+(t). \tag{19}$$

The total time dependent wave function [Eq. (8)], composed of the Gaussian wave packets, or, one may now say, composed of pairs of symmetric Gaussian wave packets, will also remain symmetric during the propagation. Projection (described in the next section) of such a wave function onto eigenstates will reveal only even components ($j = 0,2,4,...$) and no odd components ($j = 1,3,5,...$) at all. Therefore, symmetry is preserved during the H–Ne_2 collision and we will observe only even-to-even transitions for the case of symmetric molecules.

For a nonsymmetric molecule [Fig. 3(b)], the trajectories of the "+" and "−" wave packets do not follow any special rules such as those of Eq. (19); the two wave packets evolve differently under the influence of different potentials and gradients. If the initial j state is either even or odd, its symmetry is broken during the H+Ne_2 collision. As a result, the final wave function will contain both even and odd j components. So, for nonsymmetric molecules, we will observe all types of transitions: even-to-even, even-to-odd, odd-to-even, and odd-to-odd.

These properties of state-to-state transitions in this semiclassical method are equivalent to quantum selection rules. Though this idea is intuitively simple, to the best of our knowledge it has never been exploited before in a semiclassical method.

D. Analysis of the final wave function

Cross sections for state-to-state transitions, $b \leftarrow a$, are calculated semiclassically,[54]

$$\sigma_{ba} = \int_0^{2\pi} \int_0^{\infty} P_{ba}(\rho, \vartheta) \rho d\rho d\vartheta. \tag{20}$$

Here the impact parameter ρ and angle ϑ define the initial conditions for the trajectory of the H atom in a plane perpendicular to the incident direction, and $P_{ba}(\rho, \vartheta)$ is the state-to-state transition probability for such a trajectory, obtained from elements of the transition matrix,

$$P_{ba}(\rho, \vartheta) = |T_{ba}(\rho, \vartheta)|^2. \tag{21}$$

The total probability of transitions to continuum states $|k\rangle$, i.e., the dissociation probability, can be obtained from completeness,

$$P_{ka}(\rho, \vartheta) = 1 - \sum_{b=1}^{\mathcal{N}} |S_{ba}(\rho, \vartheta)|^2, \tag{22}$$

where S_{ba} are elements of the scattering matrix and the sum is over all bound states $|b\rangle$. Later in this section we derive expressions to calculate T_{ba} and S_{ba} from the results of our semiclassical method. Their dependence on ρ and ϑ is implicit and is omitted for clarity.

The scattering operator $\hat{S}$ and transition operator $\hat{T} \equiv \hat{S} - 1$ can be defined as

$$|\psi_a\rangle = \hat{S}|\phi_a\rangle, \tag{23}$$

$$|\psi_a\rangle - |\phi_a\rangle = \hat{S}|\phi_a\rangle - |\phi_a\rangle = (\hat{S} - 1)|\phi_a\rangle = \hat{T}|\phi_a\rangle. \tag{24}$$

Projecting Eq. (23) and Eq. (24) onto the final eigenstate $|b\rangle$ gives

$$\langle b|\psi_a\rangle = \langle b|\hat{S}|\phi_a\rangle = S_{ba}^{(0)}, \tag{25}$$

$$\langle b|\psi_a\rangle - \langle b|\phi_a\rangle = \langle b|\hat{T}|\phi_a\rangle = T_{ba}^{(0)}. \tag{26}$$

In our case $|\phi_a\rangle \approx |a\rangle$, so that Eqs. (25)–(26) may really be considered as approximate, "zero order" expressions. Nevertheless, for reasons discussed below (wrong asymptotic behavior and wrong relationship between transition and scattering matrices), this approximation is too crude for calculating cross sections. A more accurate formalism follows.

First, let us consider a simple case, when only $\mathcal{N}$ bound states are involved in the process (a countable, preferably small number of states). Inserting closure relations into Eq. (26) gives

$$\langle b|\psi_a\rangle - \langle b|\phi_a\rangle = \sum_{c=1}^{\mathcal{N}} \langle b|\hat{T}|c\rangle\langle c|\phi_a\rangle = \sum_{c=1}^{\mathcal{N}} T_{bc}\langle c|\phi_a\rangle. \tag{27}$$

To obtain the entire $\mathcal{N}\times\mathcal{N}$ transition matrix T_{ba} we would have to construct two $\mathcal{N}\times\mathcal{N}$ matrices $\mathbf{\Phi}$ and $\mathbf{\Psi}$ with elements defined as

$$\Psi_{ba} \equiv \langle b|\psi_a\rangle, \quad 1 \leqslant a \leqslant \mathcal{N}, \quad 1 \leqslant b \leqslant \mathcal{N}, \tag{28}$$

$$\Phi_{ca} \equiv \langle c|\phi_a\rangle, \quad 1 \leqslant a \leqslant \mathcal{N}, \quad 1 \leqslant c \leqslant \mathcal{N}, \tag{29}$$

and then to solve the matrix form of Eq. (27),

$$\mathbf{\Psi} - \mathbf{\Phi} = \mathbf{T}\mathbf{\Phi} \tag{30}$$

by inverting the $\mathbf{\Phi}$ matrix,

$$\mathbf{T} = (\mathbf{\Psi} - \mathbf{\Phi})\mathbf{\Phi}^{-1}. \tag{31}$$

Construction of the matrices $\mathbf{\Phi}$ and $\mathbf{\Psi}$ requires running $\mathcal{N}$ independent propagations, corresponding to all possible initial states $1 \leqslant a \leqslant \mathcal{N}$ in Eqs. (28)–(29). For each run, $\mathcal{N}$ projections $\langle b|\phi_a\rangle$ and $\langle b|\psi_a\rangle$ of the initial and final wave functions onto the eigenstates $1 \leqslant b \leqslant \mathcal{N}$ are calculated. Similar considerations for the scattering matrix give

$$\mathbf{S} = \mathbf{\Psi}\mathbf{\Phi}^{-1}. \tag{32}$$

This way of constructing scattering and transition matrixes is general; it does not rely on the quality of initial representation $|\psi_a\rangle$. Nevertheless, it is not straightforward to apply this procedure to the case when strong excitation is present and the continuum states $|k\rangle$ are populated during the collision, so that dissociation is induced. First of all, we want to avoid projecting onto a huge number of states $|k\rangle$ necessary to describe transitions to the continuum. Calculation of three-dimensional integrals in Eqs. (28)–(29) is the most computationally demanding part of this method; it is quite affordable when only bound states of Ne_2 are considered, but it scales as $\mathcal{N}^2$ and becomes prohibitively expensive when the number of states increases. Second, it is not clear how to apply the same semiclassical methodology when the initial state is a free continuum state $|k\rangle$. Because we want to keep our method simple, the following approach is designed to avoid starting from (and projecting onto) continuum states.

When continuum states $|k\rangle$ are involved, instead of Eq. (27) we obtain

$$\langle b|\psi_a\rangle - \langle b|\phi_a\rangle = \sum_{c=1}^{\mathcal{N}} \langle b|\hat{T}|c\rangle\langle c|\phi_a\rangle + \int_0^{\infty} \langle b|\hat{T}|k\rangle\langle k|\phi_a\rangle dk. \tag{33}$$

Rearranging terms as follows:

$$\langle b|\psi_a\rangle - \langle b|\phi_a\rangle = T_{ba}\langle a|\phi_a\rangle + \sum_{c\neq a} T_{bc}\langle c|\phi_a\rangle + \int_0^{\infty} T_{bk}\langle k|\phi_a\rangle dk, \tag{34}$$

we arrive at the general expression,

$$T_{ba} = \frac{\langle b|\psi_a\rangle - \langle b|\phi_a\rangle}{\langle a|\phi_a\rangle} - \sum_{c\neq a} T_{bc}\frac{\langle c|\phi_a\rangle}{\langle a|\phi_a\rangle} - \int_0^{\infty} T_{bk}\frac{\langle k|\phi_a\rangle}{\langle a|\phi_a\rangle} dk. \tag{35}$$

Here the sum is over all bound states, except the initial state $|a\rangle$.

The entire Eq. (35) must be used only if the initial wave function $|\phi_a\rangle$ is completely arbitrary, i.e., very different from the initial eigenstate, $|\phi_a\rangle \neq |a\rangle$. When the initial wave function is numerically exact, $|\phi_a\rangle = |a\rangle$, we can substitute $\langle a|\phi_a\rangle = 1$, $\langle b|\phi_a\rangle = \delta_{ba}$, $\langle c|\phi_a\rangle = 0$, and $\langle k|\phi_a\rangle = 0$ into Eq. (35), and obtain the expected result,

$$T_{ba} = \langle b|\psi_a\rangle - \langle b|a\rangle = \langle b|\psi_a\rangle - \delta_{ba} = S_{ba} - \delta_{ba}. \tag{36}$$

In our case $|\phi_a\rangle \approx |a\rangle$ and as the "first order" approximation to Eq. (35) we may consider

$$T_{ba}^{(1)} = \frac{\langle b|\psi_a\rangle - \langle b|\phi_a\rangle}{\langle a|\phi_a\rangle}. \tag{37}$$

Indeed, if in our case $\langle a|\phi_a\rangle \approx 1$, $\langle c|\phi_a\rangle \approx 0$ and $\langle k|\phi_a\rangle \approx 0$, then two last terms in Eq. (35), the sum and the integral, can be neglected. For the scattering matrix element we similarly obtain

$$S_{ba}^{(1)} = \frac{\langle b|\psi_a\rangle}{\langle a|\phi_a\rangle}. \tag{38}$$

Further improvement can be made by considering the relative importance of different terms in the sum and integral of Eq. (35). Note that one term in the sum, when $c = b$, corresponds to the elastic process. In the collisions we consider here, the elastic transition probabilities are much larger than inelastic ones (see Table I here and Table III in Ref. 40), so the main contribution to the sum and integral in Eq. (35) is associated with just the one term containing T_{bb}. This feature was also verified by our calculations. Therefore, the "second order" correction can be written as

$$T_{ba}^{(2)} = T_{ba}^{(1)} - T_{bb}^{(1)}\frac{\langle b|\phi_a\rangle}{\langle a|\phi_a\rangle} = \frac{\langle b|\psi_a\rangle - \langle b|\phi_a\rangle}{\langle a|\phi_a\rangle} - T_{bb}^{(1)}\frac{\langle b|\phi_a\rangle}{\langle a|\phi_a\rangle}, \quad b \neq a, \tag{39}$$

where the first order $T_{ba}^{(1)}$ and $T_{bb}^{(1)}$ are those defined by Eq. (37). This correction is applied only to inelastic processes $b \leftarrow a$, $b \neq a$ (i.e., for off-diagonal elements of the **T**-matrix), because $c \neq a$ in the sum of Eq. (35). For elastic processes $(a \leftarrow a)$ there is not a second order correction,

$$T_{aa}^{(2)} = T_{aa}^{(1)} = \frac{\langle a|\psi_a\rangle - \langle a|\phi_a\rangle}{\langle a|\phi_a\rangle} = \frac{\langle a|\psi_a\rangle}{\langle a|\phi_a\rangle} - 1. \tag{40}$$

For scattering matrix elements, we similarly obtain

$$S_{aa}^{(2)} = S_{aa}^{(1)} = \frac{\langle a|\psi_a\rangle}{\langle a|\phi_a\rangle}, \tag{41}$$

$$S_{ba}^{(2)} = S_{ba}^{(1)} - S_{bb}^{(1)} \frac{\langle b|\phi_a\rangle}{\langle a|\phi_a\rangle} = \frac{\langle b|\psi_a\rangle}{\langle a|\phi_a\rangle} - S_{bb}^{(1)} \frac{\langle b|\phi_a\rangle}{\langle a|\phi_a\rangle}, \quad b \neq a. \tag{42}$$

The "second order" expressions Eqs. (39)–(42) are still approximate, but they possess two important properties which are not present in the "zero order" expressions of Eqs. (25)–(26) or "first order" expressions Eqs. (37)–(38). The first property is the correct relationship [equivalent to that of the exact Eq. (36)] between transition and scattering matrices,

$$T_{ba}^{(2)} = S_{ba}^{(2)} - \delta_{ba}. \tag{43}$$

For elastic process $a \leftarrow a$ this property follows directly from Eq. (40) and Eq. (41). For inelastic process $b \leftarrow a$, this property can be proved by substituting Eq. (38) into Eq. (42) and Eq. (37) into Eq. (39), canceling terms and comparing results. The second property is the correct asymptotic behavior of both $S_{ba}^{(2)}$ and $T_{ba}^{(2)}$. When the impact parameter of the H–Ne_2 collision is large, $\rho \to \infty$, the H atom passes far away from the Ne_2 molecule and nothing happens. Forward–backward propagation of such a collision does not change the wave function at all: $|\psi_a\rangle = |\phi_a\rangle$. Substituting this expression into Eqs. (39)–(42) gives

$$S_{ba}^{(2)}(\rho \to \infty) = \delta_{ba}, \tag{44}$$

$$T_{ba}^{(2)}(\rho \to \infty) = 0. \tag{45}$$

Equations (44)–(45) reflect asymptotic unitarity and have the simple meaning that as $\rho \to \infty$ all inelastic transitions vanish while the elastic scattering probability approaches unity.

E. Implementation

The incident direction of H atoms is chosen to be parallel to the **Z**-axis. The center of the Ne_2 molecule is placed at the center of the reference frame. We start classical trajectories $\mathbf{R}(t)$ with the H atom placed in a plane perpendicular to the incident direction and positioned at a distance of 15 a.u. from the center of the Ne_2 molecule, so that $R_z(t=0) = -15$ a.u. Uniform Monte Carlo sampling is performed on the circle $\{0 \leqslant \rho \leqslant 15 \text{ a.u.}; 0 \leqslant \vartheta \leqslant 2\pi\}$ in this plane to choose $R_x(t=0)$ and $R_y(t=0)$. Typically, 500 trajectories are enough to calculate converged cross sections using Eq. (20) and to plot accurate opacity functions such as those in Fig. 4 below. Trajectories are propagated for 200 000 a.u. of time in both the forward and backward directions.

The required number of Gaussian wave packets, sufficient for the present task, is determined by a convergence study. Triangulation of the upper hemisphere, giving 256 surface triangles (almost three times larger than that shown in Fig. 1), is used in the final calculations. Eight Gaussian wave packets are placed along each radial direction, giving a total of 4096 Gaussians on the sphere. Although the choice of the Gaussian width parameter α in Eq. (5) is in principle arbitrary, we have studied the α-dependence of the final results for a fixed number of Gaussians used. We found that the α-dependence exhibits a plateau region, where the results are only weakly sensitive to the choice of α. We finally chose $\alpha = 0.5$, which is quite close to the center of the plateau and corresponds to a wave packet width equal to 1 a.u. Such a set of Gaussian wave packets allows us to construct quite accurate initial states $|\phi_a\rangle$ using Eq. (4). For example, when the initial eigenstate $|a\rangle$ is the ground rovibrational state ($v=0, j=0$), we obtain $\langle a|\phi_a\rangle = 0.9778$.

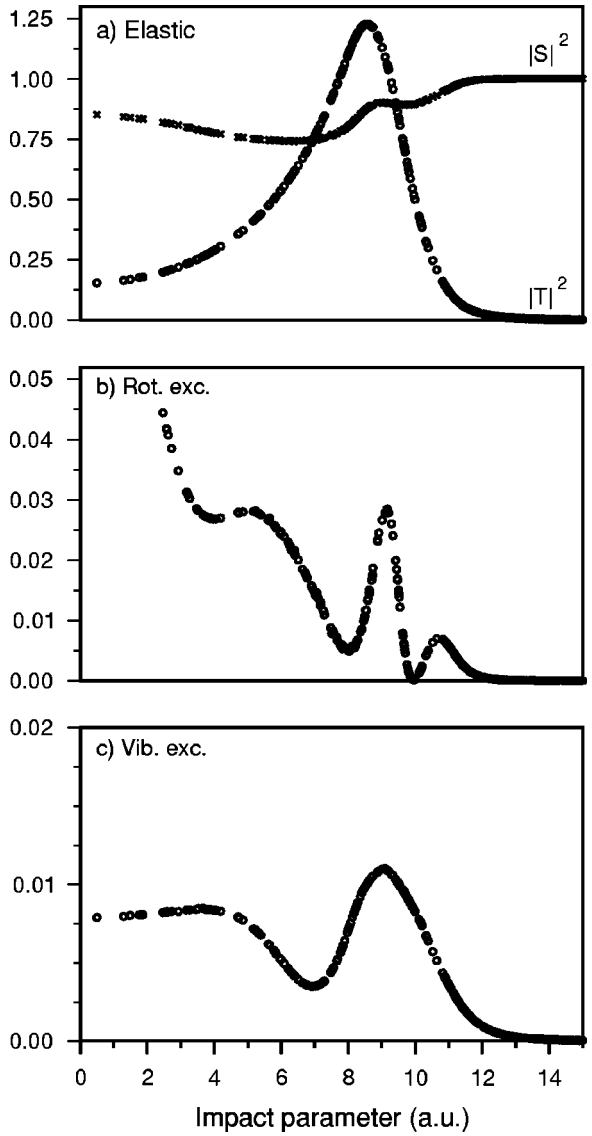

FIG. 4. Semiclassical transition and scattering probabilities for H + ^{16}Ne^{16}Ne collisions at 30 K as a function of impact parameter for (a) the elastic channel, and two inelastic channels, corresponding to (b) rotational and (c) vibrational excitations.

As it was mentioned in Ref. 41, by accurate calculations in a hyperspherical formulation we have found one extremely broad (~175 a.u.) weakly bound (−0.041 K) NeH state. In order to eliminate completely the possibility of the chaperon recombination mechanism in present model study, we decreased the mass of H atom to a 0.7 amu. That mass of the H atom, which gives no bound NeH states at all, was used in all the calculations reported herein.

IV. RESULTS AND DISCUSSION

Here we present the results in which the initial state of Ne_2 is the ground rovibrational state ($v=0, j=0$). Complete state-to-state cross section matrices (11×11 for symmetric

TABLE II. Semiclassical results. Cross sections (in a.u.) for state-to-state transitions in the Ne_2+H collision. Total energy is 30 K. Final states are labeled by v and j, vibrational and rotational quantum numbers, respectively. Initial state was ground rovibrational state ($v=0,j=0$). Shown are results for three different isotopic compositions of the Ne_2 molecule: $^{16}Ne^{16}Ne$, $^{16}Ne^{18}Ne$, and $^{18}Ne^{18}Ne$.

Final states		Isotope combinations		
v	j	16/16	16/18	18/18
0	0	243.52	242.16	241.20
	1		0.34	
	2	51.20	49.18	47.85
	3		0.22	
	4	9.60	9.34	9.20
	5		0.09	
	6	2.64	2.48	2.45
	7		0.06	
	8	0.94	0.85	0.84
	9		0.03	
	10	0.25	0.23	0.24
	11		0.01	
	12	0.05	0.05	0.05
1	0	0.54	0.50	0.48
	1		0.02	
	2	1.18	1.12	1.09
	3		0.01	
	4	0.29	0.30	0.30
	5		0.00	
	6	0.06	0.05	0.04

$^{16}Ne^{16}Ne$ and $^{18}Ne^{18}Ne$ molecules, and 20×20 for the nonsymmetric $^{16}Ne^{18}Ne$ molecule) have also been calculated using both the VRIOSA and semiclassical methods and are available from EPAPS.[55] In all cases, the total energy was 30 K ($\approx 2.59\times10^{-3}$ eV). All cross sections are summed over final m and averaged over initial m.

Semiclassical transition and scattering probabilities have been calculated as a function of the impact parameter ρ of the H atom. Results for the elastic scattering channel ($v=0,j=0)\leftarrow(v=0,j=0$) are shown in Fig. 1(a). Figures 1(b) and 1(c) illustrate our results for two inelastic transition channels: pure rotational excitation $(v=0,j=2)\leftarrow(v=0,j=0)$ and pure vibrational excitation $(v=1,j=0)\leftarrow(v=0,j=0)$, respectively. All curves exhibit the correct quantum behavior. Transition probabilities vanish, and the elastic scattering probability approaches unity as the impact parameter becomes large. This is a remarkable result, because classical scattering theory is known to fail completely in its description of elastic scattering due to the lack of phase information. Classical trajectories do not interfere with each other. Though the semiclassical Gaussian wave packets also evolve along independent, uncoupled trajectories, they nevertheless accumulate phases and contribute coherently to the overall wave function, giving rise to quantum interference.

Semiclassical state-to-state elastic and inelastic cross sections are given in Table II and can be directly compared with the VRIOSA results in Table I. One should remember that here we are comparing the results of two entirely different approximate methods, and some quantitative differences are expected and acceptable. Results in Table II show that our semiclassical method indeed captures the quantum property of symmetry—all cross sections for transitions into odd states of symmetric molecules are numerically zero (order of 10^{-32} a.u.) and are not shown. Furthermore, state-to-state cross sections for collisions involving a nonsymmetric molecules exhibit the weak selection rule seen also in Table I—transitions with even Δj are significantly more favored than transitions with odd Δj. Overall, the semiclassical and VRIOSA results are in semiquantitative agreement. Somewhat higher semiclassical cross sections, like those for $(v=1,j=2)\leftarrow(v=0,j=0)$ transitions in Table II, are due to our use of the approximate **T**-matrix in the form of Eqs. (39)–(40).

V. CONCLUSIONS

In this article we have presented the first application of a new semiclassical methodology to inelastic atom–molecule scattering in three physical dimensions. The method allows the calculation of cross sections for elastic and all inelastic state-to-state transitions, including those for long-lived quasibound states. The most important result is the demonstrated ability to build symmetry constraints into the semiclassical propagation scheme to obtain quantum selection rules. The method is attractive both for its computational affordability and the physically transparent picture it provides. Comparison of semiclassical results with quantum sudden approximation results has been done, and satisfactory agreement has been obtained.

ACKNOWLEDGMENTS

The authors acknowledge Professor Eric Heller for useful discussions. Dmitri Babikov acknowledges the Laboratory Directed Research and Development program in Los Alamos for granting a Postdoctoral Fellowship. This work was performed under the auspices of the U.S. Department of Energy under Contract No. W-7405-ENG-36.

APPENDIX A: EIGENSTATES OF Ne_2 MOLECULE

The states of the Ne_2 molecule were accurately calculated numerically. The energies E_{vj} and wave functions $\chi_{vj}(r)$ were calculated with the renormalized Numerov method.[40] The energies of long-lived states for three different isotopic compositions of Ne_2 are shown in Table III. Zero energy corresponds to the dissociation limit of Ne_2. Negative values correspond to bound states and positive values correspond to quasibound states trapped behind an angular momentum barrier. The potential energy curve for Ne–Ne interaction is very shallow ($D_e=47$ K) and it can accommodate just two vibrational and several rotational levels. As mentioned in Ref. 40, by accurate calculations in a hyperspherical formulation we have also found that $^{18}Ne_2$ possesses the $(v=2,j=0)$ state that is just barely bound at -0.00017 K. The wave function for this state extends to very large distances; a plot clearly shows that it has nonzero amplitude at distances larger than 500 a.u. It was also shown in Ref. 40 that this state should not be important for the kinetics of the recombination reaction (2). Therefore, this state has not been included into considerations in the present paper.

TABLE III. The energies (in Kelvin) of the bound and quasibound states of Ne_2. States are labeled by (v,j), vibrational and rotational quantum numbers, respectively. Shown are the results for three different isotopic compositions of Ne_2 molecule: $^{16}Ne^{16}Ne$, $^{16}Ne^{18}Ne$, and $^{18}Ne^{18}Ne$.

States		Isotope combinations		
v	j	16/16	16/18	18/18
0	0	−22.63	−23.09	−23.56
	1		−22.57	
	2	−20.99	−21.53	−22.08
	3		−19.97	
	4	−17.18	−17.91	−18.66
	5		−15.35	
	6	−11.29	−12.30	−13.34
	7		−8.79	
	8	−3.47	−4.84	−6.25
	9		−0.49	
	10	5.94	4.21	2.44
	11		9.13	
	12	16.37	14.25	12.15
1	0	−2.81	−3.20	−3.64
	1		−2.89	
	2	−1.86	−2.27	−2.73
	3		−1.37	
	4	0.17	−0.23	−0.70
	5		1.02	
	6	3.16	2.56	2.02

Symmetric molecules ($^{16}Ne^{16}Ne$ and $^{18}Ne^{18}Ne$) occur only in even j, because ^{16}Ne and ^{18}Ne are spinless bosons, and the ground electronic state of Ne_2 is a $^1\Sigma_g^+$ state. Nonsymmetric $^{16}Ne^{18}Ne$ occurs in both even and odd j. Reference 40 gives several plots of $\chi_{vj}(r)$ for one isotopic combination ($^{18}Ne^{18}Ne$) and discusses their properties in more detail.

APPENDIX B: SAMPLING THE INITIAL MOMENTA

Equations (10)–(12) may be rewritten as follows:

$$p_x^2+p_y^2+p_z^2=2\mu(E_{vj}-V(\mathbf{r})), \tag{B1}$$

$$|\mathbf{r}||\mathbf{p}|\sin\beta=\sqrt{j(j+1)}, \tag{B2}$$

$$r_x p_y - p_x r_y = m. \tag{B3}$$

Here β is an angle between vectors $\mathbf{r}$ and $\mathbf{p}$. Unknown in these three equations are only the three components of momentum vector: (p_x,p_y,p_z). Equation (B2) can be transformed into

$$\cos^2\beta=1-\frac{j(j+1)}{\mathbf{r}^2\mathbf{p}^2}. \tag{B4}$$

Then, using $r_x p_x+r_y p_y+r_z p_z=|\mathbf{r}||\mathbf{p}|\cos\beta$ it can be rewritten as

$$r_x p_x+r_y p_y+r_z p_z=\pm\sqrt{1-\frac{j(j+1)}{\mathbf{r}^2\mathbf{p}^2}}|\mathbf{r}||\mathbf{p}|. \tag{B2$'$}$$

Equations (B2$'$) and (B3) can be easily resolved to get p_x and p_y as functions of p_z. Those can be substituted in Eq. (B1), which gives four solutions:

$$p_z^{\pm\pm}=\pm\sqrt{2\mu(E_{vj}-V(\mathbf{r}))-\frac{j(j+1)}{\mathbf{r}^2}}\cdot\frac{r_z}{|\mathbf{r}|} \pm\sqrt{\frac{j(j+1)}{\mathbf{r}^2}-\frac{m^2}{r_x^2+r_y^2}}\cdot\sqrt{\frac{r_x^2+r_y^2}{\mathbf{r}^2}}, \tag{B5}$$

$$p_y^{\pm\pm}=d^{\pm}-cp_z^{\pm\pm}, \tag{B6}$$

$$p_x^{\pm\pm}=b^{\pm}-ap_z^{\pm\pm}. \tag{B7}$$

Here we defined

$$a\equiv\frac{r_x r_z}{r_x^2+r_y^2}, \tag{B8}$$

$$b^{\pm}\equiv\pm\sqrt{2\mu(E_{vj}-V(\mathbf{r}))-\frac{j(j+1)}{\mathbf{r}^2}}\cdot\frac{r_x|\mathbf{r}|}{r_x^2+r_y^2}-\frac{r_y m}{r_x^2+r_y^2}, \tag{B9}$$

$$c\equiv\frac{r_y r_z}{r_x^2+r_y^2}, \tag{B10}$$

$$d^{\pm}\equiv\pm\sqrt{2\mu(E_{vj}-V(\mathbf{r}))-\frac{j(j+1)}{\mathbf{r}^2}}\cdot\frac{r_y|\mathbf{r}|}{r_x^2+r_y^2}+\frac{r_x m}{r_x^2+r_y^2}. \tag{B11}$$

The condition

$$2\mu(E_{vj}-V(\mathbf{r}))-\frac{j(j+1)}{\mathbf{r}^2}\geqslant 0 \tag{B12}$$

in Eqs. (B5), (B9), (B11) restricts the rotational energy not to exceed the total kinetic energy. The condition;

$$\frac{j(j+1)}{\mathbf{r}^2}-\frac{m^2}{r_x^2+r_y^2}\geqslant 0 \tag{B13}$$

in Eq. (B5) restricts the energy of rotation around the Z-axis not to exceed the total rotational energy. It may be written as

$$\frac{\sqrt{r_x^2+r_y^2}}{|\mathbf{r}|}=\cos\theta\geqslant\sqrt{\frac{m^2}{j(j+1)}}, \tag{B14}$$

where θ is a spherical polar angle defined to range from $-\pi/2$ to $\pi/2$. For any m and j values this condition limits the space where the Gaussian wave packets can be placed to

$$|\theta|\leqslant\arccos\left(\sqrt{\frac{m^2}{j(j+1)}}\right). \tag{B15}$$

[1] E. J. Heller, J. Chem. Phys. **57**, 2923 (1981).
[2] M. F. Herman and E. Kluk, Chem. Phys. **91**, 27 (1984).
[3] E. Kluk, M. F. Herman, and H. L. Davis, J. Chem. Phys. **84**, 326 (1986).
[4] M. F. Herman, J. Chem. Phys. **85**, 2069 (1986).
[5] M. F. Herman, Chem. Phys. Lett. **275**, 445 (1997).
[6] B. E. Guerin and M. F. Herman, Chem. Phys. Lett. **286**, 361 (1998).
[7] M. F. Herman and D. F. Coker, J. Chem. Phys. **111**, 1801 (1999).
[8] A. R. Walton and D. E. Manolopoulos, Chem. Phys. Lett. **244**, 448 (1995).
[9] A. R. Walton and D. E. Manolopoulos, Mol. Phys. **87**, 961 (1996).
[10] M. L. Brewer, J. S. Hulme, and D. E. Manolopoulos, J. Chem. Phys. **106**, 4832 (1997).
[11] V. S. Batista and W. H. Miller, J. Chem. Phys. **108**, 498 (1997).
[12] H. Wang, D. E. Manolopoulos, and W. H. Miller, J. Chem. Phys. **115**, 6317 (2001).

[13] F. Grossmann, Phys. Rev. A **57**, 3256 (1998).
[14] F. Grossmann and A. L. Xavier, Jr., Phys. Lett. A **243**, 243 (1998).
[15] K. G. Kay, J. Chem. Phys. **100**, 4377 (1993).
[16] K. G. Kay, J. Chem. Phys. **100**, 4432 (1994).
[17] K. G. Kay, J. Chem. Phys. **101**, 2250 (1994).
[18] D. Zor and K. G. Kay, Phys. Rev. Lett. **76**, 1990 (1996).
[19] M. Madhusoodanan and K. G. Kay, J. Chem. Phys. **109**, 2644 (1998).
[20] Y. Elran and K. G. Kay, J. Chem. Phys. **114**, 4362 (2001).
[21] D. V. Shalashilin and M. S. Child, J. Chem. Phys. **113**, 10028 (2000).
[22] D. V. Shalashilin and M. S. Child, J. Chem. Phys. **115**, 5367 (2001).
[23] D. V. Shalashilin and M. S. Child, J. Chem. Phys. **114**, 9296 (2001).
[24] D. V. Shalashilin and M. S. Child, J. Chem. Phys. (unpublished).
[25] C. W. McCurdy and W. H. Miller, J. Chem. Phys. **67**, 463 (1977).
[26] M. H. Thiemens, Science **283**, 341 (1999).
[27] K. Mauersberger, B. Erbacher, D. Krankowsky, J. Gunther, and R. Nickel, Science **283**, 370 (1999).
[28] Y. Q. Gao and R. A. Marcus, Science **293**, 259 (2001); see also technical comment Science **294**, 951a (2001).
[29] Y. Q. Gao and R. A. Marcus, J. Chem. Phys. **116**, 137 (2002).
[30] C. Janssen, J. Guenther, K. Mauersberger, and D. Kranowsky, Phys. Chem. Chem. Phys. **3**, 4718 (2001).
[31] A. Gross and G. D. Billing, Chem. Phys. **217**, 1 (1997).
[32] E. A. Coronado, V. S. Batista, and W. H. Miller, J. Chem. Phys. **112**, 5566 (2000).
[33] K. G. Kay, J. Chem. Phys. **107**, 2313 (1997).
[34] M. Thoss, W. H. Miller, and G. Stock, J. Chem. Phys. **112**, 10282 (2000).
[35] V. Guallar, V. S. Batista, and W. H. Miller, J. Chem. Phys. **113**, 9510 (2000).
[36] V. Gualar, V. S. Batista, and W. H. Miller, J. Chem. Phys. **110**, 9922 (1999).
[37] R. Gelabert, X. Gimenez, M. Thoss, H. Wang, and W. H. Miller, J. Chem. Phys. **114**, 2572 (2001).
[38] H. Wang, M. Thoss, K. L. Sorge, R. Gelabert, X. Gimenez, and W. H. Miller, J. Chem. Phys. **114**, 2562 (2001).
[39] A. J. C. Varandas, A. A. C. C. Pais, J. M. C. Marques, and W. Wang, Chem. Phys. Lett. **249**, 264 (1996).
[40] R. T Pack, R. B. Walker, and B. K. Kendrick, J. Chem. Phys. **109**, 6701 (1998).
[41] R. T Pack, R. B. Walker, and B. K. Kendrick, J. Chem. Phys. **109**, 6714 (1998).
[42] See, for example, Refs. 18–22 in Ref. 40.
[43] D. Babikov, F. Aguillon, M. Sizun, and V. Sidis, Phys. Rev. A **59**, 330 (1999).
[44] G. Drolshagen and E. J. Heller, J. Chem. Phys. **82**, 226 (1985).
[45] J. R. Reimers and E. J. Heller, J. Chem. Phys. **83**, 511 (1985).
[46] J. R. Reimers and E. J. Heller, J. Chem. Phys. **83**, 516 (1985).
[47] N. E. Henriksen and E. J. Heller, Chem. Phys. Lett. **148**, 567 (1988); N. E. Henriksen and E. J. Heller, Chem Phys. Lett. **148**, 567 (1988).
[48] D. J. Tannor and D. E. Weeks, J. Chem. Phys. **98**, 3884 (1993).
[49] S. Garashchuk, Chem. Phys. Lett. **262**, 477 (1996).
[50] S. Garashchuk and D. J. Tannor, J. Chem. Phys. **110**, 2761 (1999).
[51] S. Garashchuk and J. C. Light, J. Chem. Phys. **114**, 1060 (2001).
[52] M. Thoss, H. Wang, and W. H. Miller, J. Chem. Phys. **114**, 9220 (2001).
[53] See, for example, G. Herzberg, F. R. S., in *Molecular Spectra and Molecular Structure*, 2nd ed. (Van Nostrand, New York, 1950), Vol. I, Spectra of Diatomic Molecules, Chap. I, p. 17.
[54] M. S. Child, in *Molecular Collision Theory*, edited by D. P. Craig and R. McWeeny (Academic, London, 1974), Chap. 8, p. 143.
[55] See EPAPS Document No. E-JCPSA6-117-004243 for complete state-to-state cross section matrixes, calculated using VRIOSA and semiclassical methods. A direct link to this document may be found in the online article's HTML reference section. The document may also be reached via the EPAPS homepage (http://www.aip.org/pubservs/epaps.html) or from ftp.aip.org in the directory /epaps/. See the EPAPS homepage for more information.